Optical bistability with bound states in the continuum in dielectric gratings

Dmitrii N. Maksimov,[1,2,*] Andrey A. Bogdanov,[3] and Evgeny N. Bulgakov[2,4]
[1]*Siberian Federal University, 660041 Krasnoyarsk, Russia*
[2]*Kirensky Institute of Physics, Federal Research Center KSC SB RAS, 660036 Krasnoyarsk, Russia*
[3]*Department of Physics and Engineering, ITMO University, 191002 St. Petersburg, Russia*
[4]*Reshetnev Siberian State University of Science and Technology, 660037 Krasnoyarsk, Russia*

(Received 28 May 2020; accepted 28 August 2020; published 11 September 2020)

We consider light scattering by dielectric gratings supporting optical bound states in the continuum. Due to the presence of instantaneous Kerr nonlinearity critical field enhancement in the spectral vicinity of the bound state triggers the effect of optical bistability. The onset of bistability is explained theoretically in the framework of the temporal coupled-mode theory. As the central result we cast the problem in the form of a single field-driven nonlinear oscillator. The theoretical results are verified in comparison with numerical simulations.

DOI: 10.1103/PhysRevA.102.033511

I. INTRODUCTION

Engineering high-quality resonances which provide access to tightly localized optical fields has become a topic of paramount importance in electromagnetism [1–4]. In that context, dielectric gratings are a useful optical instrument with numerous applications relying on high-quality resonances [3,5], which occur in the spectral vicinity of avoided crossings of the dielectric grating modes [6]. The utmost case of light localization is a bound state in the continuum (BIC)—an embedded state with an infinite quality factor coexisting with the scattering solutions [4,7]. Since the seminal paper by Marinica, Borisov, and Shabanov [8] BICs in all-dielectric gratings have been extensively studied both theoretically [9–14] and experimentally [15,16]. Recently, optical BICs have also been reported in hybrid photonic-plasmonic gratings [17,18].

BICs are spectrally surrounded by a leaky band of high-quality resonances which can be excited from the far zone [19]. The excitation of the strong resonances leads to critical field enhancement [20,21] with the near-field amplitude controlled by the frequency and the angle of incidence of the incoming monochromatic wave. The critical field enhancement allows for activating nonlinear optical effects even with a low amplitude of the incident waves. Such resonant enhancement of nonlinear effects may lead to the effects of symmetry breaking [22] and channel dropping [23].

Among various potential applications in nonlinear optics BICs have been used for second harmonic (SH) generation. In particular, giant conversion efficiency into the SH (up to 40%) was predicted for an array of parallel dielectric cylinders [24]. A more practical design of an AlGaAs metasurface on a quartz substrate supporting BICs was analyzed in [25], where the efficiency of SH generation $P_{2\omega}/P_{\omega}^2 \sim 10^{-2}$ W is predicted in the vicinity of a BIC. Recently, it was shown theoretically that BICs can enhance the SH convention efficiency in transition-metal dichalcogenide monolayers by more than four orders of magnitude [26]. The BIC is a dark (optically inactive) resonance which cannot be excited from the far field, however, it was shown in [27] that BICs in periodic dielectric structures can be excited by nonlinear polarization at the SH frequency induced by the incident field. The same mechanism of destructive interference underlying BICs can result in the appearance of high-quality modes in subwavelength dielectric resonators [28,29], which also demonstrate giant SH generation efficiency [30,31].

In this paper we consider the effect of critical field enhancement on the optical bistability induced by instantaneous Kerr nonlinearity. Such optical bistability emerges in the scattering spectra in the form of nonlinear Fano resonances [32,33]. Previously studies of optical bistability with BICs relied solely on either brute force numerical modeling [19,34] or the phenomenological coupled-mode approach [35]. Recently, having considered an array of nonlinear cylinders, we combined the two approaches into a single theory [36] that reduces the problem of finding the nonlinear response to solving a nonlinear coupled-mode equation for a single variable. Herewith all the parameters of the coupled-mode equation are known from solving the linear scattering problem in the spectral vicinity of the BIC, which is a far easier task than numerical modeling of nonlinear Maxwell's equation. In this paper, we present a generic theory applicable to planar structure with no mirror symmetry with respect to reflection in the plane of the structure. The theory is verified in comparison to numerical solutions of the wave equation.

II. BOUND STATES IN THE CONTINUUM

The system under consideration is shown in Fig. 1(a). It is a dielectric grating assembled of rectangular dielectric bars made of Si. The bars are periodically placed on the glass substrate. Here we only consider the scattering of TE polarized waves with the electric vector aligned with the Si bars as shown in Fig. 1. Under such conditions the propagation of electromagnetic waves is controlled by the Helmholtz

*mdn@tnp.krasn.ru

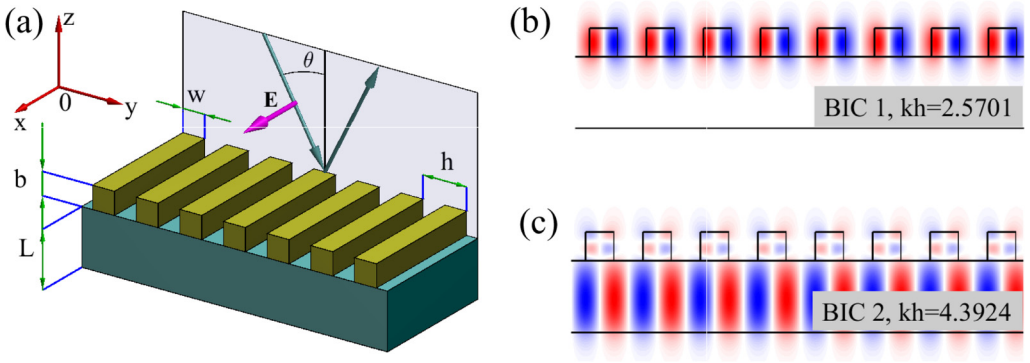

FIG. 1. (a) Dielectric grating of Si bars on a glass substrate. The plane of incidence $y0z$ is shaded gray. The magenta arrow shows the electric vector of the incident wave. The parameters are $w = 0.5h$, $b = 0.5h$, $L = 1.25h$. (b, c) Electric-field profiles of two symmetry-protected BICs visualized as E_x in the $y0z$ plane.

equation for the x component of the electric field,

$$\left(\frac{\partial^2}{\partial y^2} + \frac{\partial^2}{\partial z^2}\right)E_x + k^2\left(n_0^2 + 2n_0 n_2 |E_x|^2\right)E_x = 0, \qquad (1)$$

where k is the vacuum wave number and $n_{0,2}$ are linear and nonlinear refractive indices, respectively. In what follows the refractive index of Si is taken as $n_0 = 3.575$, and the refractive index of the substrate $n_0 = 1.5$.

Our numerical simulations using the Dirichlet-to-Neumann map method [37] have demonstrated that for the set of parameters specified in the caption to Fig. 1 the system supports two in-Γ BICs coexisting with the zeroth diffraction order. The eigenmode profiles of the BICs are shown in Figs. 1(b) and 1(c). Note the striking difference between BIC 1 and BIC 2 in Fig. 1(b) and Fig. 1(c): the field of BIC 1 is mostly localized in the Si bars, whereas the field of BIC 2 is spread across the whole grating. This difference is due to the higher eigenfrequency of BIC 2, allowing the first diffraction order in the glass substrate.

One important property of BICs is the emergence of a collapsing Fano feature in its parametric vicinity [38–42]. In this paper, we consider light scattering near the normal incidence so that the incident light couples to the band of resonant modes with a diverging Q factor as $\theta \to 0$. In Fig. 2(a) and Fig. 2(b) we show the transmittance spectra in the spectral vicinity of BIC 1 and BIC 2, correspondingly. One can see that in both cases one observes a narrow Fano feature which collapses at the exact normal incidence. There is also a difference between the two cases. Namely, there is more than a single Fano resonance at BIC 2. The transmittance exhibits two zeros and an extra peak which does not vanish at the normal incidence. This difference can be explained through the different natures of BIC 1 and BIC 2 One can see in Fig. 2 that BIC 1 occurs as an isolated resonance, while BIC 2 emerges as a result of hybridization of two resonant modes, with one of them acquiring an infinite lifetime. The latter mechanism of the BIC has been demonstrated for dielectric gratings in [11]. In the next section we provide a theoretical description of the line shapes of the Fano anomalies induced by the BICs extended to the effects of Kerr nonlinearity triggered by critical field enhancement.

III. SCATTERING THEORY

The aim of this section is to formulate the equation for the amplitude of the quasi-BIC resonant mode in the framework of the temporal coupled-mode theory (TCMT) [43]. We mention in passing that recently the TCMT approach has been revisited on mathematically rigorous grounds with application

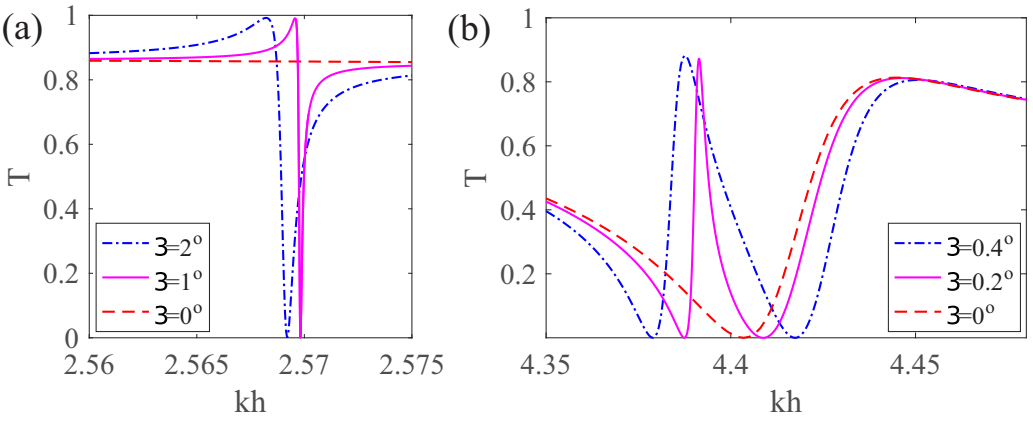

FIG. 2. (a) Transmittance spectrum in the vicinity of BIC 1 at three angles of incidence specified in the inset. (b) Transmittance spectrum in the vicinity of BIC 2 at three angles of incidence specified in the inset.

of the Feshbach projection technique [44]. The generic case of a TCMT applied to a two-dimensional structure is considered in [45]. It has been demonstrated that in the absence of mirror symmetry with respect to $y \to -y$ the application of TCMT requires consideration of four scattering channels. However, as the above symmetry holds in our case, we apply a two-channel TCMT in this paper. Following [36] we only consider the effect of a single resonant mode, mentioning in passing that a generalization of the TCMT to the multimodal case is possible [46].

A. Coupled-mode approach

Let us start with the TCMT equation for an isolated resonance [43],

$$\frac{da(t)}{dt} = i(\omega_0 - \Gamma)a + \langle d^*|s^{(+)}\rangle, \tag{2}$$

where $a(t)$ is the time-dependent amplitude of the resonant mode, ω_0 is the resonant frequency, Γ is the inverse lifetime of the resonance, $|d\rangle$ is the vector of coupling constants to the scattering channels, and $|s^{(+)}\rangle$ is the vector of incident amplitudes. In general the system under scrutiny allows for reflection at multiple Bragg's angles. The BICs in Fig. 1, however, have frequencies below the first cutoff near the normal incidence $kh < 2\pi$. In the chosen frequency range all but the zeroth diffraction channels are evanescent. So, as we stay in the domain where only specular reflection is allowed, both $|s^{(+)}\rangle = (s_1^{(+)}, s_2^{(+)})^\intercal$ and $|d\rangle = (d_1, d_2)^\intercal$ are 2×1 vectors. The subscripts 1 and 2 are applied to the upper and lower half-spaces, correspondingly. Let us, e.g., assume that a monochromatic plane wave with frequency ω is incident onto the grating from the upper half-space. The vector of the incident amplitudes is written as

$$|s^{(+)}\rangle = (\sqrt{I_0}, 0)^\intercal, \tag{3}$$

where I_0 is the flux density supported by the incident wave. After the time-harmonic substitution $a(t) = ae^{i\omega t}$ one finds

$$a = \frac{d_1\sqrt{I_0}}{[i(\omega - \omega_0) + \Gamma]}. \tag{4}$$

Finally, the outgoing amplitudes can be found from the following equation:

$$|s^{(-)}\rangle = \widehat{C} + a|d\rangle. \tag{5}$$

Here, $\widehat{C}$ is the matrix of the direct (nonresonant) process. In the case of the symmetry-protected BIC, matrix $\widehat{C}$ can be easily obtained numerically by solving the scattering problem at the normal incidence with the incident frequency equal to the BIC frequency: in other words, exactly at the point of the Fano resonance collapse [36].

The general solution of the linear scattering problem can be written through the scattering matrix $\widehat{S}(\omega)$, which links the vectors of incident and outgoing amplitudes:

$$|s^{(-)}\rangle = \widehat{S}(\omega)|s^{(+)}\rangle. \tag{6}$$

Since the system under consideration is both energy preserving and symmetric with respect to time reversal, matrices $\widehat{S}(\omega)$ and $\widehat{C}$ are simultaneously unitary and symmetric [47]. The most generic form of $\widehat{C}$ can be parameterized as

$$\widehat{C} = e^{i\phi}\begin{pmatrix} \rho e^{-i\eta} & i\tau \\ i\tau & \rho e^{i\eta} \end{pmatrix}, \tag{7}$$

where the real-valued ρ and τ are the absolute values of the reflection and transmission amplitudes, which have to satisfy the equation

$$\rho^2 + \tau^2 = 1. \tag{8}$$

Thus, taking the above into account we are left with only three independent parameters, θ, η, and ρ, which can be analytically derived from Eq. (7).

The quantities $\widehat{C}$ and $|d\rangle$ are linked through the equation [43]

$$\widehat{C}|d^*\rangle = -|d\rangle, \tag{9}$$

which is a consequence of both energy conservation and time-reversal symmetry. Equation (9) constitutes a homogeneous algebraic equation for unknown $|d\rangle$. Since the complex conjugation is involved in Eq. (9) it has to be solved for four independent variables, i.e., the real and imaginary parts of $|d\rangle$. This results in a system of four equations of rank 2. Therefore the general solution of Eq. (9) can be written as a function of two independent parameters, α and β:

$$|d\rangle = \begin{pmatrix} [\tau\alpha - i(1+\rho)\beta]e^{i\frac{\phi-\eta}{2}} \\ [\tau\beta - i(1+\rho)\alpha]e^{i\frac{\phi+\eta}{2}} \end{pmatrix}. \tag{10}$$

Note that in general $d_1 \neq d_2$. Thus, Eq. (10) takes into account the asymmetry of the coupling to the upper and lower half-spaces due to the lack of mirror symmetry in the plane of the structure [see Fig. 1(a)].

Another important relationship [43] is also a consequence of energy conservation:

$$2\Gamma = \langle d|d\rangle. \tag{11}$$

The above equation is derived by considering the decay dynamics of the system with no impinging wave. Assume that a certain amount of energy E is loaded into the resonant mode; then the solution of Eq. (2) is $a(t) = a(0)e^{i\omega_0 t - \Gamma t}$. Given that the eigenmode stores a unit energy, the energy dissipation rate can be found as

$$\frac{d\mathcal{E}}{dt} = -2\Gamma|a_0|^2, \tag{12}$$

where $\mathcal{E}$ is the energy stored in the resonant eigenmode. On the other hand, if each scattering channel attenuates a unit of energy per unit of time, Eq. (6) yields

$$\frac{d\mathcal{E}}{dt} = -\langle d|d\rangle|a_0|^2. \tag{13}$$

Combining Eqs. (12) and (13) we find Eq. (11). Note that normalization of both the eigenmode and the decay channels is important for deriving Eq. (11). Application of Eq. (11) to Eq. (10) yields

$$\alpha^2 + \beta^2 = \frac{2\Gamma}{\tau^2 + (1+\rho)^2}. \tag{14}$$

Let us summarize the findings of this subsection. First, as seen from Eq. (4) the resonant response is due to the vanishing

Γ in the denominator. Note that both Γ and ω_0 are known from the eigenmode spectrum of the grating; they can be determined as the real and imaginary parts of the resonant frequency of the leaky band host of the BIC, as done in [36]. Second, the coupling vector $|d\rangle$ is defined from the matrix of the direct process Eq. (7) via Eq. (10) up to two unknown real-valued parameters. Quite remarkable is that the presence of a symmetry-protected BIC gives easy access to the matrix of the direct process by simply computing the scattering solution at the BIC frequency and the normal incidence [36]. Finally, Eq. (14) allows for elimination of one of the free parameters, say α in Eq. (10). The remaining parameter β can be easily found by fitting the transmittance spectrum found by solving the scattering problem numerically.

B. Green's function

Let us now generalize the above result to the system with Kerr nonlinearity. In this subsection we apply the resonant-state expansion method [48] for deriving the TCMT equation taking account of nonlinearity. The key figure of merit in the resonant-state expansion method is the Green's function of the Maxwell's equations. According to [48] the spectral representation of the Green's function can be written as

$$G(\mathbf{r}', \mathbf{r}, k_0, k_y) = \sum\!\!\!\!\!\!\int_n \frac{E_x^{(n)}(\mathbf{r}, k_y)E_x^{(n)}(\mathbf{r}', -k_y)}{2k[k - k_n(k_y)]}, \tag{15}$$

where $E_x^{(n)}(\mathbf{r}, k_y)$ is the field profile of the nth resonant eigenmode and $k_n(k_y)$ is the dispersion of the resonant eigenfrequency of the leaky band in terms of the vacuum wave number, $k = \omega/c$, where c is the speed of light. The symbol $\sum\!\!\!\!\!\!\int_n$ is used for the combined contribution of a discrete sum and integration along the cuts. For the spectral representation of Eq. (15) to be valid the eigenfields $E_x^{(n)}(\mathbf{r}, k_y)$ must obey the normalization condition

$$1 + \delta_{0,k_n} = I_n^V + \lim_{k\to k_n} \frac{S_n^{\partial V}}{k^2 - k_n^2} \tag{16}$$

with

$$I_n^V = \int_V dV E_x^{(n)}(\mathbf{r}, -k_y)E_x^{(n)}(\mathbf{r}', k_y) \tag{17}$$

and

$$S_n^{\partial V} = \oint_{\partial V} dS\big[E_x^{(n)}(\mathbf{r}, -k_y)\partial_S \tilde{E}_x^{(n)}(\mathbf{r}', k_y, k) - \tilde{E}_x^{(n)}(\mathbf{r}, -k_y, k)\partial_S E_x^{(n)}(\mathbf{r}', k_y)\big], \tag{18}$$

where ∂_S is used for the normal derivative with respect to the boundary of the elementary cell and $\tilde{E}_z^{(n)}(\mathbf{r}', k_y, k_0)$ is the analytic continuation of the eigenfield in the vicinity of its resonant eigenfrequency such that

$$E_x^{(n)}(\mathbf{r}', k_y) = \lim_{k\to k_n} \tilde{E}_x^{(n)}(\mathbf{r}', k_y, k). \tag{19}$$

C. Resonant approximation

To establish a link between the resonant-state expansion and the single-mode TCMT we apply the resonant approximation, i.e., in Eq. (15) we retain only the term with $k - k_n(k_y)$ in the denominator. All the other terms are assumed to be independent of the frequency on the scale of the narrow Fano feature induced by the BIC. In terms of the TCMT the nonresonant terms are accumulated in the direct process. The resulting resonant Green's function is simply

$$G^{(\mathrm{res})}(\mathbf{r}', \mathbf{r}') = \frac{E_x^{(0)}(\mathbf{r}, k_y)E_x^{(0)}(\mathbf{r}', -k_y)}{2k[k - k(k_x)]}, \tag{20}$$

where $E_x^{(0)}(\mathbf{r}, k_y)$ is the profile of the resonant eigenmode. Above we have omitted the band index of the dispersion $k(k_x)$ bearing in mind that the resonant approximation uses the dispersion and the mode profiles of the BIC host band.

First, let us again consider the linear scattering problem. As before we assume that a TE polarized plane wave with intensity I_0 impinges onto the structure at the near-normal incidence. Then, solving Eq. (1) with the resonant Green's function, Eq. (20), one finds

$$E_x = \frac{\sqrt{I_0}E_x^{(0)}(\mathbf{r}, k_y)}{2k[k - k(k_y)]} \int_V dV E_x^{(0)}(\mathbf{r}', -k_y)J(\mathbf{r}'), \tag{21}$$

where the source term can be expressed through the incident field $E_x^{(\mathrm{in})}$ as

$$J = -\left(\frac{\partial^2}{\partial y^2} + \frac{\partial^2}{\partial z^2}\right)E_x^{(\mathrm{in})} - n_0^2 E_x^{(\mathrm{in})}, \tag{22}$$

where $E_x^{(\mathrm{in})}$ is normalized to carry a unit of energy per unit of time across the boundary of the scattering domain. Thus, the amplitude of the physical incident wave is only controlled by I_0.

To be consistent with the resonant approximation we also assume that the near-field response is dominated by the quasi-BIC eigenmode

$$E_x = \frac{1}{\sqrt{A}} a E_x^{(0)}, \tag{23}$$

where A is the normalization constant. Substituting the above equation into Eq. (21) one finds

$$a = \frac{\sqrt{I_0 A}}{2k[k - k(k_x)]} \int_V dV E_x^{(0)}(\mathbf{r}', -k_y)J(\mathbf{r}'). \tag{24}$$

Comparing Eqs. (4) and (24) one finds

$$d_1 = \frac{i\sqrt{A}c}{2k} \int_V dV E_x^{(0)}(\mathbf{r}', -k_y)J(\mathbf{r}'), \tag{25}$$

where c is the speed of light. The above equation is difficult to apply in computations, since it requires the explicit analytic form of the leaky mode profiles under the normalization condition, Eq. (16). We, however, know from the previous subsection how d_1 can be found from the scattering spectra with the use of Eqs. (10) and (14).

D. Nonlinear case

Now let us generalize the above result to the nonlinear case. After taking the same route we end up with the equation for a

$$a + \mathcal{J}\frac{n_0 n_2 k}{A[k - k(k_y)]}|a|^2 a = \frac{\sqrt{I_0}d_1}{ic[k - k(k_y)]}, \tag{26}$$

where

$$\mathcal{J} = \int_{V_{\text{nlin}}} dV E_x^{(0)}(-k_y) E_x^{(0)}(k_y) \left| E_x^{(0)}(k_y) \right|^2, \tag{27}$$

and the integration is performed only over the domain with a nonlinear refractive index V_{nlin}. Finally, note that $\mathcal{J}$ must be parabolic in k_y, since the problem is symmetric with respect to the angle of incidence. Therefore we drop the dependence on k_y using the field profile at the Γ point, i.e., the BIC

$$\mathcal{J} = \int_{V_{\text{nlin}}} dV \left| E_x^{(\text{BIC})} \right|^4 + O\left(k_y^2\right) \tag{28}$$

since the BIC profile is a well-behaved function decaying with the distance from the grating. Following [49] one easily finds that Eq. (16) is equivalent to the integration over z from $+\infty$ to $-\infty$:

$$1 = \int_{-\infty}^{\infty} dV n_0^2 \left| E_x^{(\text{BIC})} \right|^2. \tag{29}$$

Importantly, Eq. (29) does not contain surface terms and, thus, can be easily implemented in simulations taking into account that the BIC decays exponentially with $|z| \to \infty$. Finally, note that the integral in Eq. (29) is equal to twice the electromagnetic energy stored in the BIC. Thus, to be consistent with Eq. (11) we set $A = 2$.

E. Nonlinear temporal coupled-mode equation

Now, in accordance with Eq. (26) the final result reads

$$[i(\omega - \omega_0) + \Gamma]a + i\frac{\mathcal{J}}{2} n_0 n_2 \omega |a|^2 a = \sqrt{I_0} d_1. \tag{30}$$

Equation (30) differs from Eq. (4) only by the presence of the nonlinear term proportional to J. This means that to describe the nonlinear response in the spectral vicinity of a BIC it is sufficient to know the solution of the linear problem including the field profile of the BIC. Once the BIC field profile is known it can be substituted into Eq. (28) to find $\mathcal{J}$. The nonlinear Eq. (30) can then be solved for the response in the frequency domain.

It is remarkable that the nonlinear correction in Eq. (30) exactly coincides with that obtained previously with the perturbation theory [50]. Note, however, that the results reported in [50] were obtained under the assumption of smallness of the nonlinear term. Another issue with straightforward application of the perturbation theory is the normalization condition of the unperturbed eigenmodes. The formal solution presented in [50] involves integration across the whole space which is impossible due to divergence of the resonant eigenmodes in the far zone [51]. As one can see from the previous subsection the normalization issue can only be easily resolved in the spectral vicinity of a BIC.

Finally, in the time domain Eq. (30) can be replaced by

$$\frac{d}{dt}\left(a + \frac{\mathcal{J}}{2} n_0 n_2 |a|^2 a\right) = (i\omega_0 - \Gamma)a + \sqrt{I_0} d_1 e^{i\omega t}. \tag{31}$$

The time-harmonic solutions of the above equations can be tested for stability by series expansions with respect to small perturbations as explained in [36].

IV. NUMERICAL VALIDATION

In this section we apply our previous findings to the scattering spectra. To obtain the matrices of the direct process we numerically solved the linear scattering problem at exact normal incidence with the vacuum wave number of the incident wave equal to that of the BIC. For BIC 1 the matrix of the direct process has been found as

$$\hat{C}_{\text{BIC1}} = \begin{pmatrix} -0.3753 + 0.0494i & -0.8834 + 0.2765i \\ -0.8833 + 0.2765i & 0.3365 - 0.1734i \end{pmatrix}, \tag{32}$$

while for BIC 2 the numbers are

$$\hat{C}_{\text{BIC2}} = \begin{pmatrix} -0.9333 - 0.1121i & 0.0768 - 0.3323i \\ 0.0768 - 0.3323i & -0.8879 - 0.3086i \end{pmatrix}. \tag{33}$$

In the next step the numerical values of the three remaining parameters, ω_0, Γ, and α, were evaluated by fitting to the scattering spectra in Fig. 2 at different angles of incidence. The effective nonlinearity coefficient was found with Eq. (28) by integrating the BIC profiles shown in Figs. 1(b) and 1(c). The results are listed in Table I. In Table I we also present the ratio of the absolute values of the coupling constants d_1 and d_2. One can see that in both cases the coupling to the lower half-space is somewhat larger than that to the upper half-space, $|d_1| < |d_2|$.

To obtain the nonlinear scattering spectra, Eq. (1) was solved numerically using the pseudospectral method [52]. In our simulations we took $n_2 = 5 \times 10^{-18}$ m^2/W, which corresponds to silicon at 1.8 μm [53]. The results are plotted in Fig. 3 in comparison with the numerical solution of Eq. (30). The intensities of the incident waves are given in the caption to Fig. 3. First, one can see in Figs. 3(a) and 3(b) that there is a reasonably good agreement between the TCM and the numerical spectra for BIC 1. The agreement can be made perfect by slightly tuning α and/or $\mathcal{J}$. For BIC 2, however, the agreement is not that good and our theory can only provide a rough estimate of the parameter values leading to optical bistability. The discrepancy is due to the single-mode approximation, which is not capable of accounting for all features of the BIC emerging with an avoided crossing. To highlight the

TABLE I. List of the TCMT parameters.

	θ	$h\omega_0/c$	$h\Gamma/c$	α (p.d.u.)	$\lvert d_1/d_2 \rvert$	$\mathcal{J}$ (p.d.u.)
BIC 1	1°	2.5670	0.065×10^{-5}	6.24×10^{-3}	0.907	3.04×10^{-2}
BIC 1	2°	2.5689	0.031×10^{-3}	1.23×10^{-2}	0.914	3.04×10^{-2}
BIC 2	0.2°	4.39074	1.59×10^{-3}	9.05×10^{-2}	0.717	3.79×10^{-4}

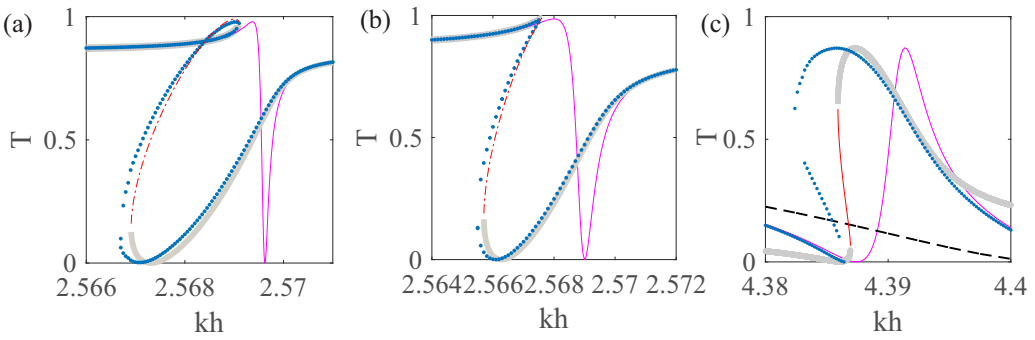

FIG. 3. Bistability in transmittance spectra. (a) BIC 1, $\theta = 1^{\circ}$, $I_0 = 1.82 \times 10^5$ MW/m^2. (b) BIC 1, $\theta = 2^{\circ}$, $I_0 = 8.39 \times 10^5$ MW/m^2. (c) BIC 2, $\theta = 0.2^{\circ}$, $I_0 = 3.92 \times 10^8$ MW/m^2. Thin magenta lines demonstrate Fano resonances unperturbed by the nonlinearity. Blue dots represent numerical solutions obtained with the pseudospectral method. Stable solutions of Eq. (30) are shown by thick gray lines. Thin red lines show unstable solutions of Eq. (30). The dashed black line in (c) shows the transmittance at exact normal incidence.

limitations of the single-mode TCMT in Fig. 3(c) we plotted the transmittance at the normal incidence. One can easily see that the transmittance at the normal incidence is dependent on the frequency, whereas the single-mode TCMT assumes that it is constant. On the other hand, even the single-mode approximation manages to grasp the major feature of BIC 2 with respect to initiating bistability. One can see in Table I that the effective nonlinearity coefficient $\mathcal{J}$ is two orders of magnitude smaller with BIC 2 than with BIC 1. The reason for this is clearly shown in Figs. 1(b) and 1(c): the field of BIC 1 is concentrated about the nonlinear medium (silicon bars), while for BIC 2 the field is evenly spread across the whole grating. The small value of $\mathcal{J}$ results in very high intensities needed to trigger optical bistability. This rules out the application of BIC 2 in a realistic experiment.

V. SUMMARY AND CONCLUSIONS

In this paper we have considered the effect of optical bistability induced by bound states in the continuum (BICs) in dielectric gratings. We proposed a coupled-mode approach which leads to a single nonlinear equation for the amplitude of the resonant eigenmode of the BIC host band. It is shown how all parameters entering the nonlinear coupled-mode equation can be evaluated from the solution of the linear scattering problem.

We believe that the approach presented here can be of use in engineering photonic systems with a resonantly enhanced nonlinear response, as the coupled-mode equation is much easier to solve than nonlinear Maxwell's equations. At the same time our approach provides a clue for choosing the type of BIC in order to maximize the nonlinear effect. Namely, it has been shown that BICs with a frequency lower than the first diffraction order in the substrate are better for activating nonlinearity.

On the other hand, from the fundamental viewpoint we have seen that the scattering of light in the spectral vicinity of a BIC can be handled by the resonant-state expansion method [48]. This naturally prompts us to extend the theory for the two-mode case, which potentially leads to an intricate interplay between the BICs and the other mode with a finite lifetime that can be excited from the far zone even at the normal incidence [35]. The application of resonant-state expansion to finite-lived states would, however, require introducing the analytical continuation normalization condition, Eq. (19), to eigenmodes that are known only numerically. We speculate that the above problem would be an interesting topic for future studies.

ACKNOWLEDGMENTS

This work was financially supported by the Government of the Russian Federation through the ITMO Fellowship and Professorship Program. A.A.B. also acknowledges support by the Ministry of Science and Higher Education of Russian Federation, goszadanie No. 2019-1246 and RFBR (18-32-20205).

[1] S. John, Why trap light? Nat. Mater. **11**, 997 (2012).
[2] D. Marpaung, C. Roeloffzen, R. Heideman, A. Leinse, S. Sales, and J. Capmany, Integrated microwave photonics, Laser Photon. Rev. **7**, 506 (2013).
[3] P. Qiao, W. Yang, and C. J. Chang-Hasnain, Recent advances in high-contrast metastructures, metasurfaces, and photonic crystals, Adv. Opt. Photon. **10**, 180 (2018).
[4] C. W. Hsu, Bo Zhen, A. D. Stone, J. D. Joannopoulos, and M. Soljačić, Bound states in the continuum, Nat. Rev. Mater. **1**, 16048 (2016).
[5] C. J. Chang-Hasnain and W. Yang, High-contrast gratings for integrated optoelectronics, Adv. Opt. Photon. **4**, 379 (2012).
[6] V. Karagodsky, C. Chase, and C. J. Chang-Hasnain, Matrix Fabry–Perot resonance mechanism in high-contrast gratings, Opt. Lett. **36**, 1704 (2011).
[7] K. Koshelev, G. Favraud, A. Bogdanov, Y. Kivshar, and A. Fratalocchi, Nonradiating photonics with resonant dielectric nanostructures, Nanophotonics **8**, 725 (2019).
[8] D. C. Marinica, A. G. Borisov, and S. V. Shabanov, Bound States in the Continuum in Photonics, Phys. Rev. Lett. **100**, 183902 (2008).
[9] F. Monticone and A. Alù, Bound states within the radiation continuum in diffraction gratings and the role of leaky modes, New J. Phys. **19**, 093011 (2017).

[10] E. N. Bulgakov, D. N. Maksimov, P. N. Semina, and S. A. Skorobogatov, Propagating bound states in the continuum in dielectric gratings, J. Opt. Soc. Am. B **35**, 1218 (2018).
[11] E. N. Bulgakov and D. N. Maksimov, Avoided crossings and bound states in the continuum in low-contrast dielectric gratings, Phys. Rev. A **98**, 053840 (2018).
[12] S.-G. Lee and R. Magnusson, Band dynamics of leaky-mode photonic lattices, Opt. Express **27**, 18180 (2019).
[13] D. A. Bykov, E. A. Bezus, and L. L. Doskolovich, Coupled-wave formalism for bound states in the continuum in guided-mode resonant gratings, Phys. Rev. A **99**, 063805 (2019).
[14] X. Gao, B. Zhen, M. Soljačić, H. Chen, and C. W. Hsu, Bound states in the continuum in fiber bragg gratings, ACS Photon. **6**, 2996 (2019).
[15] Z. F. Sadrieva, I. S. Sinev, K. L. Koshelev, A. Samusev, I. V. Iorsh, O. Takayama, R. Malureanu, A. A. Bogdanov, and A. V. Lavrinenko, Transition from optical bound states in the continuum to leaky resonances: Role of substrate and roughness, ACS Photon. **4**, 723 (2017).
[16] H. Hemmati and R. Magnusson, Resonant dual-grating metamembranes supporting spectrally narrow bound states in the continuum, Adv. Opt. Mater. **7**, 1900754 (2019).
[17] S. I. Azzam, V. M. Shalaev, A. Boltasseva, and A. V. Kildishev, Formation of Bound States in the Continuum in Hybrid Plasmonic-Photonic Systems, Phys. Rev. Lett. **121**, 253901 (2018).
[18] R. Kikkawa, M. Nishida, and Y. Kadoya, Polarization-based branch selection of bound states in the continuum in dielectric waveguide modes anti-crossed by a metal grating, New J. Phys. **21**, 113020 (2019).
[19] L. Yuan and Y. Y. Lu, Strong resonances on periodic arrays of cylinders and optical bistability with weak incident waves, Phys. Rev. A **95**, 023834 (2017).
[20] J. W. Yoon, S. H. Song, and R. Magnusson, Critical field enhancement of asymptotic optical bound states in the continuum, Sci. Rep. **5**, 18301 (2015).
[21] V. Mocella and S. Romano, Giant field enhancement in photonic resonant lattices, Phys. Rev. B **92**, 155117 (2015).
[22] E. Bulgakov, K. Pichugin, and A. Sadreev, Symmetry breaking for transmission in a photonic waveguide coupled with two off-channel nonlinear defects, Phys. Rev. B **83**, 045109 (2011).
[23] E. Bulgakov, K. Pichugin, and A. Sadreev, Channel dropping via bound states in the continuum in a system of two nonlinear cavities between two linear waveguides, J. Phys.: Condens. Matter **25**, 395304 (2013).
[24] F. R. Ndangali and S. V. Shabanov, The resonant nonlinear scattering theory with bound states in the radiation continuum and the second harmonic generation, in *Active Photonic Materials V*, Vol. 8808 (International Society for Optics and Photonics, Bellingham, WA, 2013), p. 88081F.
[25] K. Koshelev, A. Bogdanov, and Y. Kivshar, Meta-optics and bound states in the continuum, Sci. Bull. **64**, 836 (2019).
[26] T. Wang and S. Zhang, Large enhancement of second harmonic generation from transition-metal dichalcogenide monolayer on grating near bound states in the continuum, Opt. Express **26**, 322 (2018).
[27] L. Yuan and Y. Y. Lu, Excitation of bound states in the continuum via second harmonic generations, SIAM J. Appl. Math. **80**, 864 (2020).
[28] M. V. Rybin, K. L. Koshelev, Z. F. Sadrieva, K. B. Samusev, A. A. Bogdanov, M. F. Limonov, and Y. S. Kivshar, High-q Supercavity Modes in Subwavelength Dielectric Resonators, Phys. Rev. Lett. **119**, 243901 (2017).
[29] A. A. Bogdanov, K. L. Koshelev, P. V. Kapitanova, M. V. Rybin, S. A. Gladyshev, Z. F. Sadrieva, K. B. Samusev, Y. S. Kivshar, and M. F. Limonov, Bound states in the continuum and fano resonances in the strong mode coupling regime, Adv. Photon. **1**, 016001 (2019).
[30] L. Carletti, K. Koshelev, C. De Angelis, and Y. Kivshar, Giant Nonlinear Response at the Nanoscale Driven by Bound States in the Continuum, Phys. Rev. Lett. **121**, 033903 (2018).
[31] K. Koshelev, S. Kruk, E. Melik-Gaykazyan, J.-H. Choi, A. Bogdanov, H.-G. Park, and Y. Kivshar, Subwavelength dielectric resonators for nonlinear nanophotonics, Science **367**, 288 (2020).
[32] A. E. Miroshnichenko, S. F. Mingaleev, S. Flach, and Y. S. Kivshar, Nonlinear Fano resonance and bistable wave transmission, Phys. Rev. E **71**, 036626 (2005).
[33] S. P. Shipman and S. Venakides, An exactly solvable model for nonlinear resonant scattering, Nonlinearity **25**, 2473 (2012).
[34] L. Yuan and Y. Y. Lu, Diffraction of plane waves by a periodic array of nonlinear circular cylinders, Phys. Rev. A **94**, 013852 (2016).
[35] S. D. Krasikov, A. A. Bogdanov, and I. V. Iorsh, Nonlinear bound states in the continuum of a one-dimensional photonic crystal slab, Phys. Rev. B **97**, 224309 (2018).
[36] E. N. Bulgakov and D. N. Maksimov, Nonlinear response from optical bound states in the continuum, Sci. Rep. **9**, 7153 (2019).
[37] Y. Huang and Y. Y. Lu, Scattering from periodic arrays of cylinders by Dirichlet-to-Neumann maps, J. Lightwave Technol. **24**, 3448 (2006).
[38] C. S. Kim, A. M. Satanin, Y. S. Joe, and R. M. Cosby, Resonant tunneling in a quantum waveguide: Effect of a finite-size attractive impurity, Phys. Rev. B **60**, 10962 (1999).
[39] S. P. Shipman and S. Venakides, Resonant transmission near nonrobust periodic slab modes, Phys. Rev. E **71**, 026611 (2005).
[40] A. F. Sadreev, E. N. Bulgakov, and I. Rotter, Bound states in the continuum in open quantum billiards with a variable shape, Phys. Rev. B **73**, 235342 (2006).
[41] C. Blanchard, J.-P. Hugonin, and C. Sauvan, Fano resonances in photonic crystal slabs near optical bound states in the continuum, Phys. Rev. B **94**, 155303 (2016).
[42] E. N. Bulgakov and D. N. Maksimov, Optical response induced by bound states in the continuum in arrays of dielectric spheres, J. Opt. Soc. Am. B **35**, 2443 (2018).
[43] S. Fan, W. Suh, and J. D. Joannopoulos, Temporal coupled-mode theory for the Fano resonance in optical resonators, J. Opt. Soc. Am. A **20**, 569 (2003).
[44] M. Makarenko, A. Burguete-Lopez, F. Getman, and A. Fratalocchi, Generalized Maxwell projections for multi-mode network photonics, Sci. Rep. **10**, 9038 (2020).
[45] H. Zhou, B. Zhen, C. W. Hsu, O. D. Miller, S. G. Johnson, J. D. Joannopoulos, and M. Soljačić, Perfect single-sided radiation and absorption without mirrors, Optica **3**, 1079 (2016).
[46] W. Suh, Z. Wang, and S. Fan, Temporal coupled-mode theory and the presence of non-orthogonal modes in lossless

multimode cavities, IEEE J. Quantum Electron. **40**, 1511 (2004).

[47] Z. Zhao, C. Guo, and S. Fan, Connection of temporal coupled-mode-theory formalisms for a resonant optical system and its time-reversal conjugate, Phys. Rev. A **99**, 033839 (2019).

[48] T. Weiss, M. Schäferling, H. Giessen, N. A. Gippius, S. G. Tikhodeev, W. Langbein, and E. A. Muljarov, Analytical normalization of resonant states in photonic crystal slabs and periodic arrays of nanoantennas at oblique incidence, Phys. Rev. B **96**, 045129 (2017).

[49] P. S. Pankin, D. N. Maksimov, K.-P. Chen, and I. V. Timofeev, Fano feature induced by a bound state in the continuum via resonant state expansion, Sci. Rep. **10**, 13691 (2020).

[50] J. Bravo-Abad, S. Fan, S. G. Johnson, J. D. Joannopoulos, and M. Soljacic, Modeling nonlinear optical phenomena in nanophotonics, J. Lightwave Technol. **25**, 2539 (2007).

[51] P. Lalanne, W. Yan, K. Vynck, C. Sauvan, and J.-P. Hugonin, Light interaction with photonic and plasmonic resonances, Laser Photon. Rev. **12**, 1700113 (2018).

[52] L. Yuan and Y. Y. Lu, Efficient numerical method for analyzing optical bistability in photonic crystal microcavities, Opt. Express **21**, 11952 (2013).

[53] Y. Yue, L. Zhang, H. Huang, R. G. Beausoleil, and A. E. Willner, Silicon-on-nitride waveguide with ultralow dispersion over an octave-spanning mid-infrared wavelength range, IEEE Photon. J. **4**, 126 (2012).